


Hybrid Kohn-Sham + Thomas-Fermi scheme for high-temperature density functional theory

P. Hollebon¹* and T. Sjoström¹

Theoretical Division, Los Alamos National Laboratory, Los Alamos, New Mexico 87545, USA

 (Received 23 August 2021; revised 1 June 2022; accepted 2 June 2022; published 13 June 2022)

Density functional theory has revolutionised our understanding of dense, strongly coupled systems in the condensed-matter limit. At elevated temperatures, such as those found in warm dense matter and dense plasma, the computational cost of calculating enough states to accurately describe a thermal ensemble of electrons is a major obstacle to practical Kohn-Sham calculations. This problem has recently been tackled from a number of approaches, including a plane-wave approximation for electrons at high energy. In this work, we demonstrate how the Thomas-Fermi density of states, equivalent to a local plane-wave approximation, can yield improved results for thermodynamic quantities, electron density profiles, and interatomic forces while requiring fewer states than existing methods.

DOI: [10.1103/PhysRevB.105.235114](https://doi.org/10.1103/PhysRevB.105.235114)

I. INTRODUCTION

Our understanding of warm and hot dense matter (WDM and HDM) rests in no small part on our capacity to perform accurate, large-scale (both spatially and temporally) quantum-mechanical simulations. In turn this provides insight into properties ranging from bulk thermodynamic quantities [1,2] to the detailed microphysics of dense plasmas, with applications in environments as diverse as the interiors of stars to inertial confinement fusion experiments here on Earth. These unique conditions of high density and temperature create a challenging quantum many-body problem. Consequently, a large number of approaches and computational techniques are available to tackle the problem [3–6].

The choice of approach is frequently influenced not only by the inherent approximations, but also by the available computational resources and time. For example, while Kohn-Sham density functional theory (KS-DFT) [7–9] has proven to be a powerful tool for ground-state and WDM conditions, it becomes computationally prohibitive for larger systems and at higher temperatures [10]. Other methods, such as the path-integral Monte Carlo method [11], can benefit from an increased efficiency at higher temperatures while encountering other challenges in the condensed limit. There exists, therefore, a significant motivation to extend practical implementations of these methods across the temperature-density plane in order to test their underlying approximations.

In this paper, we consider a hybrid DFT approach suitable for high temperatures in which the electronic structure is partitioned into Kohn-Sham and Thomas-Fermi (TF) contributions. A similar, extended plane-wave approximation (extPW) [12] has recently been proposed and used to perform high-temperature DFT calculations, with favorable comparison to full Kohn-Sham calculations. By comparison, our TF-based model bridges the gap to standard orbital-free DFT methods [1,2,13,14], and it is shown here to yield improved results when compared to extPW calculations.

As a test case, we perform calculations for iron under WDM and HDM conditions using our own implementation of both the extPW method and our TF-based model in QUANTUM ESPRESSO. Our method demonstrates approximately one order of magnitude improvement in pressure calculations over the extPW method, as well as significantly better electron density profiles and interatomic forces due to our account of the nonuniform potential distribution in a plasma.

In addition, we have supplemented our iron results with calculations for a disordered ion arrangement of warm dense lithium deuteride (LiD). Both the extPW method and our TF-based model yield excellent results for the pressure, however the latter is seen to yield notably more accurate predictions for interatomic forces.

II. METHOD

In a hybrid DFT approach, the equilibrium density of the system is partitioned into Kohn-Sham $n_{\text{KS}}(\mathbf{r})$ and orbital-free contributions $n_{\text{of}}(\mathbf{r})$ [10]. The former is found from a reduced Kohn-Sham calculation in which one solves for a limited number of Kohn-Sham states ψ_i^{KS} , $i = 1, \dots, N$:

$$\left[\frac{-\hbar^2}{2m_e} \nabla^2 + v_{\text{eff}} \right] \psi_i^{\text{KS}} = \epsilon_i^{\text{KS}} \psi_i^{\text{KS}}. \quad (1)$$

The Kohn-Sham density contribution is then found by weighting the Kohn-Sham states according to Fermi-Dirac distribution:

$$n_{\text{KS}}(\mathbf{r}) = \sum_i^N \frac{2}{1 + e^{\beta(\epsilon_i^{\text{KS}} - \mu)}} |\psi_i^{\text{KS}}(\mathbf{r})|^2, \quad (2)$$

where μ is the chemical potential of the system and $\beta = 1/k_B T$. In addition, we have included the factor of 2 for spin degeneracy as we neglect fine-structure effects for the purposes of studying WDM and HDM conditions.

At high temperatures, the number of states needed to calculate the density solely in terms of the Kohn-Sham wave functions scales as $T^{3/2}$ [15]. Consequently, standard Kohn-Sham algorithms exhibit cubic scaling in computational cost

*phollebon@lanl.gov

with temperature at a fixed system size. Hybrid schemes, therefore, use an alternative means to determine the remaining contribution $n_{\text{of}}(\mathbf{r})$. Once this is achieved for the noninteracting problem, described by Eq. (1), the usual mixing algorithms for obtaining a self-consistent density in DFT can be used.

In this work, we use a TF form for the density of states such that one has

$$n_{\text{of}}^{\text{TF}}(\mathbf{r}) = \frac{\sqrt{8m^3}}{\pi^3 \hbar^3} \int_{\epsilon_{\text{KS}}}^{\infty} d\epsilon [\epsilon - v(\mathbf{r})]^{1/2} f_{\text{FD}}(\epsilon), \quad (3)$$

where $f_{\text{FD}}(\epsilon)$ is the Fermi-Dirac distribution without spin degeneracy. The key difference between our method and that of the extended plane-wave approach is the use of a spatially varying potential $v(\mathbf{r})$. The method of Ref. [12] is then recovered by setting this to a constant $v(\mathbf{r}) = U_0$.

Our prior rationale for using Eq. (3) is based on the understanding that, in expanding the density matrix at finite temperature, both the density and kinetic energy (or equivalently, the pressure) can be approximated at zeroth-order using a local Thomas-Fermi form. The associated errors in the local density of states are then proportional to the (local) gradients of the potential over kinetic energy or, for the case of integrated quantities, over the temperature [16,17]. While such an expansion in terms of the potential can be mathematically difficult for general potentials in three dimensions, including those with strong gradients such as Coulomb potentials, their resummations in terms of the density are the basis for many OF-DFT calculations today [18–21]. In this paper, we aim to demonstrate via example how a TF-based approximation can also function well in a hybrid scheme, in which some subsection of the density of states is described by Kohn-Sham orbitals.

There remains the task of determining an appropriate v_r . This is particularly relevant for integration with codes that make heavy use of nonlocal pseudopotentials, upon which the majority of KS-DFT calculations in WDM and hot dense plasma conditions have relied. For the calculations presented in this paper, we will simply take the local component of the effective potential v_{eff} appearing in Eq. (1). By comparison, in Ref. [12], U_0 is suggested to be determined by fitting to N_{av} states at the high-energy end of the density of states given by Eq. (1), i.e.,

$$U_0 = \frac{1}{N} \sum_{i=N_{\text{KS}}-N_{\text{av}}}^{N_{\text{KS}}} \epsilon_i^{\text{KS}} - \left\langle \psi_i^{\text{KS}} \left| \frac{-\hbar^2}{2m_e} \nabla^2 \right| \psi_i^{\text{KS}} \right\rangle. \quad (4)$$

This approach implicitly accounts for the nonlocal component of the Kohn-Sham potential V_{eff} . However, our calculations have shown this nonlocal component to have only a minor impact, consistent with Ref. [12]. Indeed, for the pseudopotentials used in this work, an equally effective value for U_0 is provided by simply taking the spatial average of the local potential across the system. This may not hold for all pseudopotentials, in particular those with very deep cores, however a spatial average of the potential has proven to be a reasonable approximation thus far [22]. As an alternative to Eq. (4), it also enables us to consider especially low values for the number of Kohn-Sham states N_{KS} as well as avoiding oscillations in the value of U_0 as one varies N_{av} .

We end this section by noting that taking the local component of v_{eff} is not the only way to determine $v(\mathbf{r})$ in Eq. (3), and one could equally introduce a constant offset from nonlocal potential contributions or use a local form of the averaging in Eq. (4). In the following section, we will justify our local-only approximation *a posteriori* by showing that the nonlocal contributions to high-energy Kohn-Sham states remain small in comparison.

III. COMPUTATIONAL DETAILS

We perform calculations using both the extended plane-wave method of Ref. [12] and our TF-based approach under WDM conditions with comparison to full KS-DFT results. Calculations are performed using the QUANTUM ESPRESSO package [23–25] modified to include these two methods. In addition, we have made some minor changes to convergence criteria of the code that may affect those looking to reproduce our results. Both criteria must be satisfied simultaneously for the code to stop.

First, the convergence of our self-consistent field (SCF) calculation is determined by the *density residual* between the electron density $n_{\text{in}}(\mathbf{r})$ used to generate the Kohn-Sham potential and the total density $n_{\text{out}}(\mathbf{r})$ obtained from Eqs. (2) and (3). The threshold is set such that we require

$$\int d^3\mathbf{r} |n_{\text{in}}(\mathbf{r}) - n_{\text{out}}(\mathbf{r})|^2 \leq 10^{-13}. \quad (5)$$

Second, convergence of the Kohn-Sham wave functions is determined by the *wave-function residual* when solving Eq. (1). For a Kohn-Sham Hamiltonian \hat{H} and overlap operator \hat{S} associated with the pseudopotential, convergence is determined by the condition

$$\langle \psi_i^{\text{KS}} | [\hat{H} - \epsilon_i^{\text{KS}} \hat{S}]^2 | \psi_i^{\text{KS}} \rangle \leq \sigma_{\psi}. \quad (6)$$

The value of σ_{ψ} varies depending on the occupation of the state $|\psi_i^{\text{KS}}\rangle$. For those with occupation numbers greater than 10^{-3} , $\sigma_{\psi} = 10^{-14}$, while for those with lower occupation numbers we have a less strict setting of $\sigma_{\psi} = 10^{-6}$. To achieve these levels of wave-function convergence, a buffer zone of 3 (forcibly unoccupied) bands is used for $20 < N_{\text{KS}} \leq 100$, 10 for $100 < N_{\text{KS}} \leq 500$, and 15 for $N_{\text{KS}} > 500$.

Evaluating the orbital-free contributions to the density and pressure requires the efficient computation of numerous incomplete Fermi-Dirac integrals (see the Appendix). For this purpose, we use the highly efficient algorithm 745 [26,27]. To accelerate our calculations, we have made additional, minor modifications to QUANTUM ESPRESSO. The chemical potential μ is determined via a simple Newton-Raphson approach, as opposed to the original bisection algorithm, and a starting guess is provided by the chemical potential from the previous SCF cycle.

Our calculations for bcc iron ($\rho = 8.18 \text{ g cm}^{-3}$) utilize a two-atom unit cell with a plane-wave cutoff of 150 Ry and a shifted $8 \times 8 \times 8$ Monkhorst-Pack grid to sample the Brillouin zone. Force calculations for iron were performed using a 64-atom disordered liquid configuration at the Γ point with a plane-wave cutoff of 200 Ry. All results for iron use a 16-electron projector augmented wave pseudopotentials generated via ATOMPAW [28] together with the

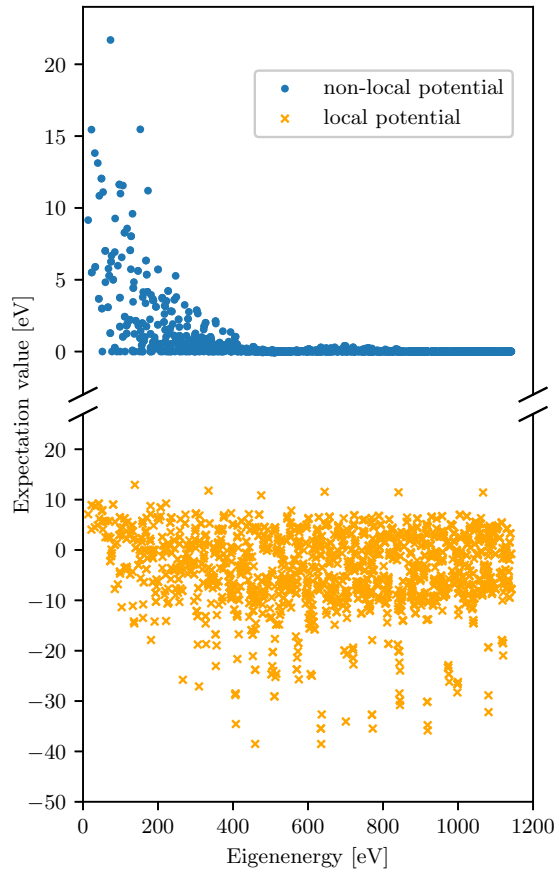


FIG. 1. Contributions from the local and nonlocal potential to each Kohn-Sham eigenvalue for bcc iron at $T_e = 60$ eV.

Perdew-Burke-Ernzerhof generalized gradient approximation for the exchange-correlation potential.

Calculations for warm dense LiD were performed using a disordered eight-atom unit at a density of 0.825 g cm^{-3} . A plane-wave cutoff of 200 Ry and a shifted $4 \times 4 \times 4$ Monkhorst-Pack grid were used. Pseudopotentials were the precision Li and H potentials available from the Standard Solid-State Pseudopotentials library [29,30]. The exchange-correlation potential used was the Perdew-Burke-Ernzerhof generalized gradient approximation.

IV. RESULTS

A. Warm dense Fe

We present calculations for warm dense iron at electronic temperatures of $T_e = 20, 40,$ and 60 eV using both our TF-based model and the extPW approach. As previously described in Sec. II, we have neglected the role of the nonlocal potential in the TF contribution. The appropriateness of this approximation is shown in Fig. 1, in which we plot the contribution of the local and nonlocal potential for eigenvalues of the bcc lattice at $T_e = 60$ eV. It is clear from the plot that for higher energies, the average expectation value of the nonlocal component becomes negligible much faster [12] than one can reasonably approximate the local potential as a constant. For bulk properties such as the equation of state, therefore, we

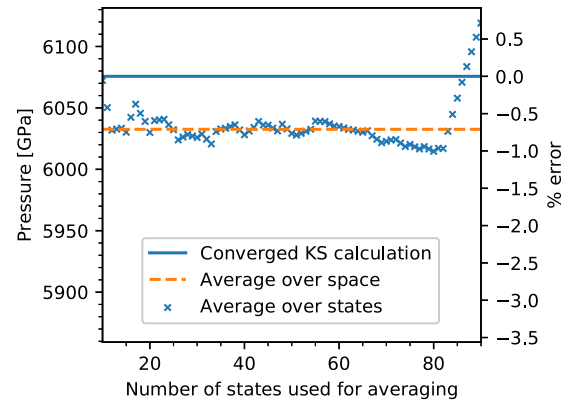


FIG. 2. Predicted pressure for bcc iron ($T_e = 60$ eV, $N_{KS} = 100$) using the extPW method as N_{av} in Eq. (4) is varied. The pressure is seen to oscillate around that obtained using a spatially averaged potential.

expect a proper account of the spatially varying local potential to be more important than the nonlocal potential.

In Fig. 2 we plot extPW results for the pressure ($T_e = 60$ eV) as the number of Kohn-Sham states used to determine U_0 is varied [see Eq. (4)]. The fluctuations are small up to $N_{av} = 80$, at which point the averaging method begins to include states that straddle the line between bound and free. Otherwise, the pressure is seen to fluctuate within a fraction of a percent around an equivalent calculation for which U_0 taken as the spatial-mean of the local potential. In principle, the number N_{av} might be chosen in an attempt to minimize error with respect to a full Kohn-Sham calculation; however, it is not immediately clear if determining an optimal N_{av} with small-scale calculations will scale appropriately to large molecular-dynamics simulations. In any case, the percentage error is far from a smooth function of N_{av} , and for the sake of definiteness we perform the following extPW calculations using the spatial-mean definition for U_0 .

In Figs. 3 and 4 we compare the extPW method and our TF-based approach to fully converged Kohn-Sham pressure calculations for a bcc lattice configuration at elevated electron temperatures. In each case, our method shows up to an order of magnitude less error when only a few Kohn-Sham states are included. As the number of Kohn-Sham states is increased, both models show a significant reduction in error; however, the progression becomes somewhat erratic beyond about 0.1%. There are multiple possible reasons for the less than regular progression shown in Fig. 4 as the number of Kohn-Sham state is increased. First, both methods use a sharp transition from the Kohn-Sham to the orbital-free density of states, and the latter is inevitably not quite continuous with the former. Second, both the extPW method and TF-based model are effectively completely sampling the Brillouin zone in contrast to the approximate Monkhorst-Pack sampling used for the Kohn-Sham contributions. Overall, we have checked the convergence of our Kohn-Sham calculations with respect to k -point sampling and plane-wave cutoffs to an accuracy of 0.01%. However, there remains the possibility of some unusual convergence behavior when Brillouin zone sampling of the density of states is not identical for all energies.

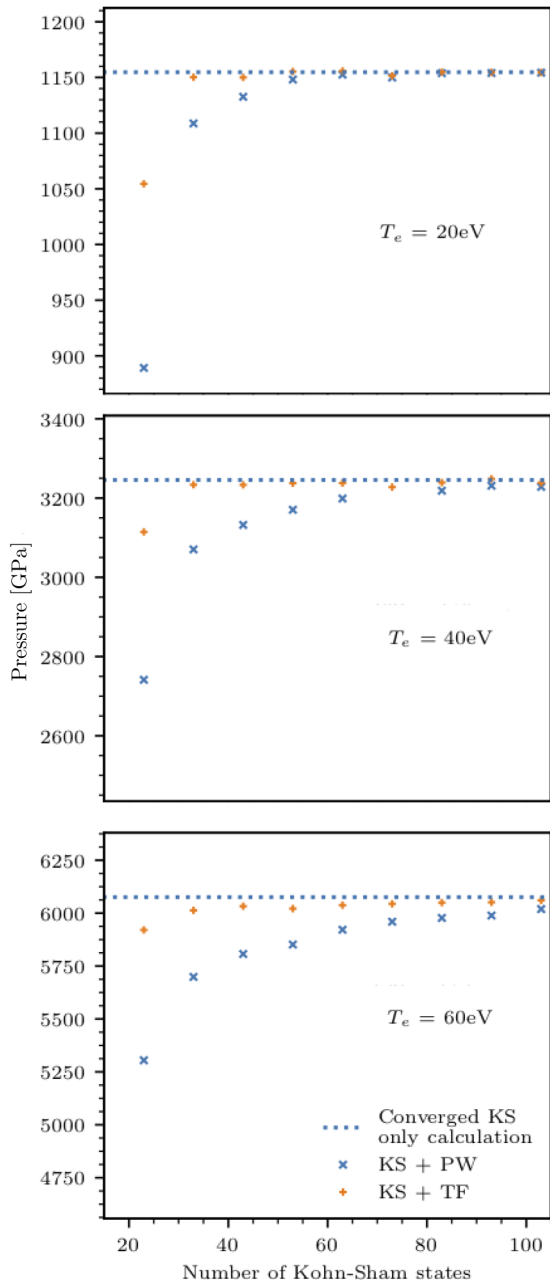


FIG. 3. Shown are the calculated pressures via the method of this paper (KS + TF), the extPW scheme (KS + PW), and a full Kohn-Sham calculation for bcc iron.

Figure 5 shows the percentage error in valence electron density of both methods for a bcc lattice configuration (viewed along the 111 direction) at $T_e = 60$ eV. Our results indicate that the TF-type model is the more favorable approximation in this regime. The mean error using the extPW method is 9%, almost twice that of our approach at 4.7%, while the maximum error is also greater at 19.3% compared to 11.9%.

Finally, we show in Fig. 6 the root-mean-squared (RMS) absolute and percentage errors in interatomic forces for a disordered liquid configuration of 64 iron atoms at $T_e = 20$ eV. Forces are calculated via electrostatics from the total density $n_{\text{KS}} + n_{\text{of}}$ in the same manner as a standard Kohn-Sham calculation, i.e., under the approximation that the hybrid ap-

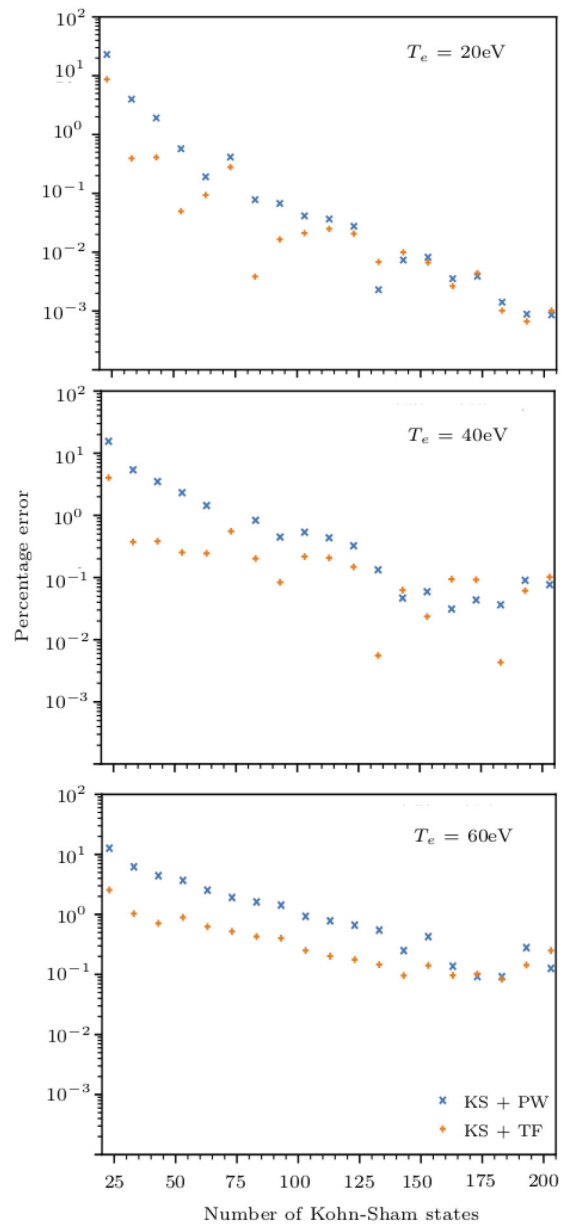


FIG. 4. Plotted are the percentage errors for both the extPW method (KS + PW) and the TF-based scheme (KS + TF) relative to a full Kohn-Sham calculation for bcc iron.

proximation yields the same density as a full Kohn-Sham calculation. The TF-based approach continues to show an improvement over the extPW approximation, with the uniform orbital-free density component of the latter not contributing to the forces due to translational symmetry.

B. Warm dense LiD

We supplement the above results with a further test calculation for warm dense LiD at $T_e = 40$ eV. Figure 7 shows the error in the static pressure (i.e., discounting thermal ion motion) and the RMS error in forces for an eight-atom disordered configuration. A full Kohn-Sham calculation yielded a static pressure of 401 GPa. Both the extPW and TF-based approach provide extremely accurate values for the pressure

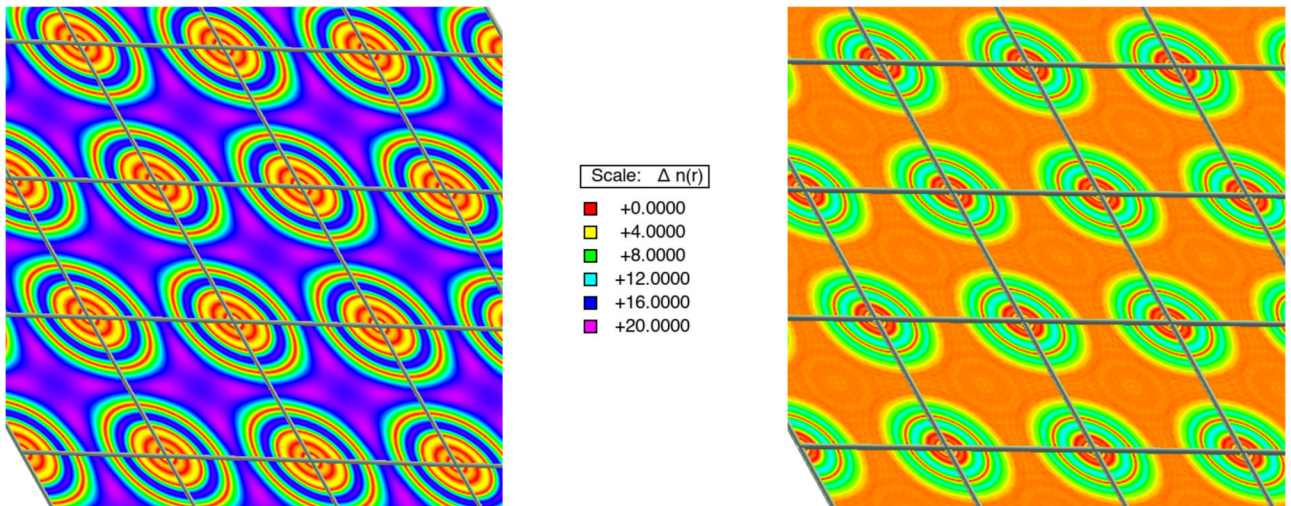


FIG. 5. Percentage error in the electron density relative to a full Kohn-Sham calculation, as viewed along the 111 direction in bcc iron ($\rho = 8.18 \text{ g cm}^{-3}$, $T_e = 60 \text{ eV}$). The results of this work (right) using a hybrid TF-based model show significantly less error compared to the extended plane-wave method (left).

with a relative error of $\sim 0.025\%$. However, the approach of this paper remains the more accurate one for calculating interatomic forces.

V. CONCLUSIONS

In this work, we have introduced a hybrid TF-based scheme to extend Kohn-Sham calculations to high temperatures, and we implemented it within the QUANTUM ESPRESSO code. Our method presented here complements multiple avenues of inquiry, all with the common goal of efficient and accurate high-temperature DFT calculations. Importantly, the work presented here makes contact with the more standard orbital-free calculations for which the TF model is frequently the zeroth-order approximation.

As an example, we have presented calculations for iron under WDM to HDM conditions with favorable comparison to full Kohn-Sham calculations. In particular, we

find an approximate order-of-magnitude increase in accuracy for the pressure when compared with existing plane-wave methods, as well as much improved results for the electron density profile and interatomic forces. These results are supplemented with a calculation for disordered LiD at $T_e = 40 \text{ eV}$. While both the extTF and TF-based approaches yield accurate results for the pressure, the latter is able to predict interatomic forces with notably more accuracy.

The calculation of properties beyond bulk thermodynamic quantities, such as ionization cross sections and dynamic transport coefficients, is particularly sensitive to plasma inhomogeneities and the subsequent effect on scattering processes. In this work, the TF form for the local density of states begins to account for these spatial variations in a very basic way while also serving as a starting point for further refinements, the incorporation of which is the focus of current and future research.

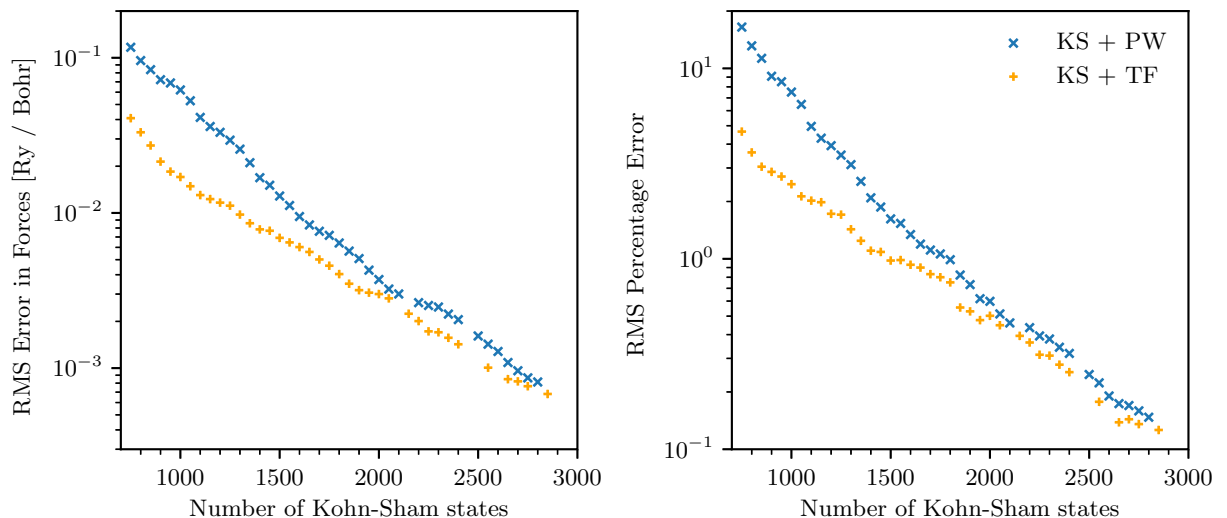


FIG. 6. Root mean squared (RMS) absolute and percentage errors for forces acting on a disordered system of 64 iron atoms at $T_e = 20 \text{ eV}$.

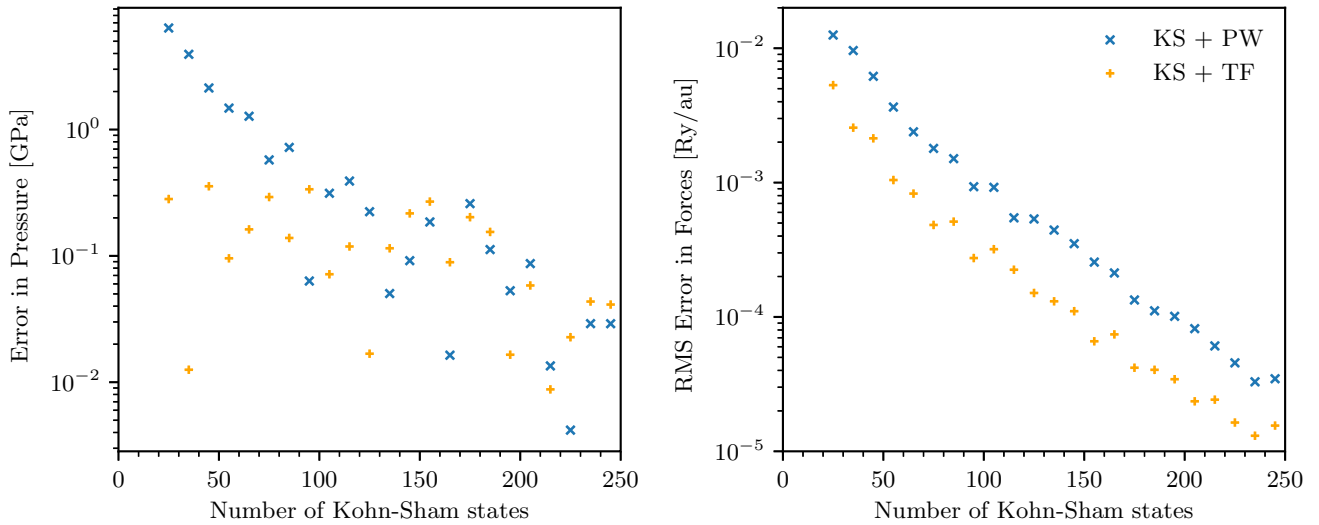


FIG. 7. Results for a disordered ion configuration of LiD at $T_e = 40$ eV and a density of 0.825 g cm^{-3} . Plotted are the absolute errors for pressure and forces calculated using both the TF-based approach and extPW method relative to a fully converged Kohn-Sham calculation.

ACKNOWLEDGMENTS

Research presented in this article was supported by the Laboratory Directed Research and Development program of Los Alamos National Laboratory under Project No. 20180613-ECR.

APPENDIX: THERMODYNAMIC EXPRESSIONS

Our orbital-free contribution to the density [Eq. (3)] utilizes a Thomas-Fermi-like local density of states:

$$\text{LDOS}(\mathbf{r}, \epsilon) = \frac{\sqrt{8m^3}}{\pi^3 \hbar^3} [\epsilon - v(\mathbf{r})]^{1/2}. \quad (\text{A1})$$

The orbital-free contribution to thermodynamic quantities then generalizes from the usual Thomas-Fermi expressions in a manner analogous to Eq. (3):

$$E^{\text{TF}} = \int d^3\mathbf{r} \int_{\epsilon_N^{\text{KS}}}^{\infty} d\epsilon \text{LDOS}(\mathbf{r}, \epsilon) \epsilon f_{\text{FD}}(\epsilon),$$

$$P^{\text{TF}} = \frac{1}{3V} \int d^3\mathbf{r} \int_{\epsilon_N^{\text{KS}}}^{\infty} d\epsilon \text{LDOS}(\mathbf{r}, \epsilon) [\epsilon - v(\mathbf{r})] f_{\text{FD}}(\epsilon),$$

$$S^{\text{TF}} = -k_B \int d^3\mathbf{r} \int_{\epsilon_N^{\text{KS}}}^{\infty} d\epsilon \text{LDOS}(\mathbf{r}, \epsilon) \times \{f_{\text{FD}}(\epsilon) \ln f_{\text{FD}}(\epsilon) + [1 - f_{\text{FD}}(\epsilon)] \ln[1 - f_{\text{FD}}(\epsilon)]\}. \quad (\text{A2})$$

-
- [1] T. Sjostrom, S. Crockett, and S. Rudin, Multiphase aluminum equations of state via density functional theory, *Phys. Rev. B* **94**, 144101 (2016).
- [2] T. Sjostrom and S. Crockett, Quantum molecular dynamics of warm dense iron and a five-phase equation of state, *Phys. Rev. E* **97**, 053209 (2018).
- [3] W.-D. Kraeft, D. Kremp, W. Ebeling, and G. Röpke, *Quantum Statistics of Charged Particle Systems* (Akademie-Verlag, Berlin, 1986).
- [4] M. W. Dharma-wardana, Current issues in finite-T density-functional theory and warm-correlated matter, *Computation* **4**, 16 (2016).
- [5] M. Bonitz, Z. A. Moldabekov, and T. S. Ramazanov, *Phys. Plasmas* **26**, 090601 (2019).
- [6] B. Larder, D. O. Gericke, S. Richardson, P. Mabey, T. G. White, and G. Gregori, Fast nonadiabatic dynamics of many-body quantum systems, *Sci. Adv.* **5**, eaaw1634 (2019).
- [7] P. Hohenberg and W. Kohn, Inhomogeneous electron gas, *Phys. Rev.* **136**, B864 (1964).
- [8] W. Kohn and L. J. Sham, Self-consistent equations including exchange and correlation effects, *Phys. Rev.* **140**, A1133 (1965).
- [9] N. D. Mermin, Thermal properties of the inhomogeneous electron gas, *Phys. Rev.* **137**, A1441 (1965).
- [10] A. J. White and L. A. Collins, Fast and Universal Kohn-Sham Density Functional Theory Algorithm for Warm Dense Matter to Hot Dense Plasma, *Phys. Rev. Lett.* **125**, 055002 (2020).
- [11] K. P. Driver and B. Militzer, All-Electron Path Integral Monte Carlo Simulations of Warm Dense Matter: Application to Water and Carbon Plasmas, *Phys. Rev. Lett.* **108**, 115502 (2012).
- [12] S. Zhang, H. Wang, W. Kang, P. Zhang, and X. T. He, Extended application of Kohn-Sham first-principles molecular dynamics method with plane wave approximation at high energy: From cold materials to hot dense plasmas, *Phys. Plasmas* **23**, 042707 (2016).
- [13] V. V. Karasiev, T. Sjostrom, and S. B. Trickey, Generalized-gradient-approximation noninteracting free-energy functionals for orbital-free density functional calculations, *Phys. Rev. B* **86**, 115101 (2012).

- [14] V. V. Karasiev, T. Sjoström, and S. B. Trickey, Finite-temperature orbital-free DFT molecular dynamics: Coupling profess and quantum espresso, *Comput. Phys. Commun.* **185**, 3240 (2014).
- [15] A. Blanchet, M. Torrent, and J. Clérouin, Requirements for very high temperature Kohn-Sham DFT simulations and how to bypass them, *Phys. Plasmas* **27**, 122706 (2020).
- [16] D. Kirzhnits, Quantum corrections to the Thomas-Fermi equation, *Sov. Phys. JETP* **5**, 64 (1957).
- [17] W. C. Witt and E. A. Carter, Kinetic energy density of nearly free electrons. I. Response functionals of the external potential, *Phys. Rev. B* **100**, 125106 (2019).
- [18] M. Durand, M. Brack, and P. Schuck, A semiclassical density matrix valid beyond the classically allowed region, *Z. Phys. A* **286**, 381 (1978).
- [19] M. Durand and P. Schuck, Partial resummation of \hbar -expansion of the Bloch density for non local potentials, *Z. Phys. A* **296**, 87 (1980).
- [20] A. Cangi, E. K. Gross, and K. Burke, Potential functionals versus density functionals, *Phys. Rev. A* **88**, 062505 (2013).
- [21] A. Sergeev, R. Jovanovic, S. Kais, and F. H. Alharbi, On the divergence of gradient expansions for kinetic energy functionals in the potential functional theory, *J. Phys. A* **49**, 285202 (2016).
- [22] A. Blanchet, J. Clérouin, M. Torrent, and F. Soubiran, Extended first-principles molecular dynamics model for high temperature simulations in the Abinit code: Application to warm dense aluminum, *Comput. Phys. Commun.* **271**, 108215 (2022).
- [23] P. Giannozzi, S. Baroni, N. Bonini, M. Calandra, R. Car, C. Cavazzoni, D. Ceresoli, G. L. Chiarotti, M. Cococcioni, I. Dabo, A. Dal Corso, S. De Gironcoli, S. Fabris, G. Fratesi, R. Gebauer, U. Gerstmann, C. Gougoussis, A. Kokalj, M. Lazzeri, L. Martin-Samos, *et al.*, QUANTUM ESPRESSO: A modular and open-source software project for quantum simulations of materials, *J. Phys.: Condens. Matter* **21**, 395502 (2009).
- [24] P. Giannozzi Jr., O. Andreussi, T. Brumme, O. Bunau, M. Buongiorno Nardelli, M. Calandra, R. Car, C. Cavazzoni, D. Ceresoli, M. Cococcioni, N. Colonna, I. Carnimeo, A. D. Corso, S. de Gironcoli, P. Delugas, R. A. DiStasio Jr., A. Ferretti, A. Floris, G. Fratesi, G. Fugallo, *et al.*, Advanced capabilities for materials modelling with Quantum ESPRESSO, *J. Phys.: Condens. Matter* **29**, 465901 (2017).
- [25] P. Giannozzi, O. Baseggio, P. Bonfà, D. Brunato, R. Car, I. Carnimeo, C. Cavazzoni, S. De Gironcoli, P. Delugas, F. Ferrari Ruffino, A. Ferretti, N. Marzari, I. Timrov, A. Urru, and S. Baroni, Quantum ESPRESSO toward the exascale, *J. Chem. Phys.* **152**, 154105 (2020).
- [26] M. Goano, Algorithm 745: Computation of the complete and incomplete Fermi-Dirac integral, *ACM Trans. Math. Softw.* **21**, 221 (1995).
- [27] M. Goano, Remark on algorithm 745, *ACM Trans. Math. Softw.* **23**, 295 (1997).
- [28] N. A. W. Holzwarth, A. R. Tackett, and G. E. Matthews, A Projector Augmented Wave (PAW) code for electronic structure calculations, Part I: Atompaw for generating atom-centered functions, *Comput. Phys. Commun.* **135**, 329 (2001).
- [29] K. Lejaeghere, G. Bihlmayer, T. Björkman, P. Blaha, S. Blügel, V. Blum, D. Caliste, I. E. Castelli, S. J. Clark, A. D. Corso, S. de Gironcoli, T. Deutsch, J. K. Dewhurst, I. D. Marco, C. Draxl, M. Dułak, O. Eriksson, J. A. Flores-Livas, K. F. Garrity, L. Genovese, *et al.*, Reproducibility in density functional theory calculations of solids, *Science* **351**, aad3000 (2016).
- [30] G. Prandini, A. Marrazzo, N. Mounet, and N. Marzari, Precision and efficiency in solid-state pseudopotential calculations, *npj Comput. Mater.* **4**, 72 (2018).